

RESEARCH ARTICLE | MAY 23 2024

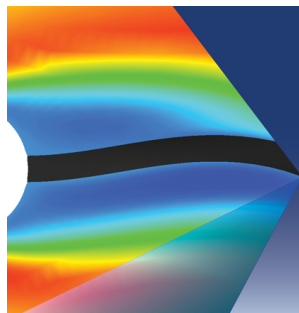
Vibration-triggered spreading of nanofluid drops

Schon Fusco ; Lingyue Liu (刘凌岳) ; Miguel Ángel Cabrerizo-Vilchez; Erin Koos ; Miguel Ángel Rodríguez-Valverde  



Physics of Fluids 36, 052014 (2024)

<https://doi.org/10.1063/5.0205785>



Physics of Fluids

Special Topic:

Fluid-Structure Interaction

Guest Editors: A-Man Zhang, Tiegang Liu, Boo Cheong Khoo and Nhan Phan-Thien

[Submit Today!](#)

Vibration-triggered spreading of nanofluid drops

Cite as: Phys. Fluids **36**, 052014 (2024); doi: 10.1063/5.0205785

Submitted: 28 February 2024 · Accepted: 8 May 2024 ·

Published Online: 23 May 2024



View Online



Export Citation



CrossMark

Schon Fusco,¹ Lingyue Liu (刘凌岳),² Miguel Ángel Cabrerizo-Vilchez,¹ Erin Koos,²
and Miguel Ángel Rodríguez-Valverde^{1,a)}

AFFILIATIONS

¹Department of Applied Physics, Laboratory of Surface and Interface Physics, University of Granada, 18071 Granada, Spain

²Department of Chemical Engineering, Soft Matter, Rheology and Technology, KU Leuven, 3001 Leuven, Belgium

^{a)} Author to whom correspondence should be addressed: marodri@ugr.es

ABSTRACT

This study explores the effects of nanoparticles on the dynamics of drop spreading under external vibration, presenting an advance in the understanding of nanofluid behavior on vibrating substrates. This work introduces insights into nanoparticle-mediated drop spreading, offering implications for improving particulate coatings, mini-mixers, and particle segregation technologies. By employing a twofold approach that combines oscillating drop dynamics with internal flow pattern analysis, we find how even small concentrations of hydrophilic or hydrophobized silica nanoparticles inside water sessile droplets significantly alter the spreading process on silanized glass surfaces. Our study allows distinct drop spreading regimes to be identified based on nanoparticle concentration and vibration amplitude, for both hydrophilic and hydrophobized nanoparticles. Through a comprehensive analysis, we demonstrate that the vibration-triggered spreading of nanofluids can lead to a stable and controlled manipulation of complex liquids.

© 2024 Author(s). All article content, except where otherwise noted, is licensed under a Creative Commons Attribution (CC BY) license (<https://creativecommons.org/licenses/by/4.0/>). <https://doi.org/10.1063/5.0205785>

I. INTRODUCTION

Vibration has been demonstrated to influence liquid drop behavior on solid surfaces. Numerous studies have reported that an external oscillating field allows single drops to be controlled, leading to phenomena like the transition from a Wenzel wetting state to the Cassie-Baxter state,¹ net drop motion,² or drop relaxation.³ Knowledge from drop vibrations can be applied to various technological fields such as mixing,⁴ drop segregation,^{5,6} and surface cleaning.⁷ Recent research efforts have focused on the spreading phenomena induced by oscillating mechanical field such as vibration and ultrasound.^{6,8,9} Vibrations are able to mitigate hysteresis¹⁰ and to induce oscillation in contact lines.¹¹ The effects of vibration on pure water drops are well known, but there is a lack of knowledge on the dynamics of drops containing finely dispersed particles, i.e., nanofluid drops, stimulated by mechanical vibration. This excitation can lead to exploitable phenomena such as particle patterning^{12–14} and particle size sorting.¹⁵

Nanoparticles (NPs) suspended in water sessile drops are known for their ability to influence wetting properties and to promote spreading.^{16,17} Contact line dynamics are often altered by concentration gradients of the NPs driven by internal flows¹⁸ due to convection, collective diffusion,¹⁹ or disjoining pressure.²⁰ Monitoring the flow fields developed within nanofluid drops allows the particular NP

dynamics to be understood, which is required to identify the role of NPs in inducing and controlling drop spreading.

To investigate the interconnected effects of NP suspensions on drop spreading, we performed experiments with pure water and nanofluid sessile drops on a non-wetting substrate under in-plane vibrations. The purely sinusoidal signal was produced at a fixed frequency for different amplitudes ranging from 20 to 160 μm (approximately 0.8%–6% of the drop contact length). These experiments were conducted with hydrophilic and hydrophobized silica NPs at concentrations of 0.1 and 1 vol. %. To obtain a holistic picture of the vibration-induced drop spreading, we employed a twofold approach by studying both the oscillating drop dynamics and the internal flow patterns with fluorescent NPs. We focused on the early stages of the vibration experiments and rationalized the phenomenon in terms of a driven oscillator with varying solid–liquid stiffness.

II. MATERIALS AND METHODS

A. Nanofluids

Stable aqueous suspensions of hydrophilic (ζ -potential: -44.93 ± 0.09 mV) and hydrophobized (ζ -potential: -35.80 ± 0.22 mV) 150 nm fluorescent core-shell silica NPs were synthesized using a modified Stöber synthesis following the procedure of Liu *et al.*²¹ where the

cores consist of silica labeled with rhodamine B isothiocyanate (RBITC, Sigma-Aldrich) and the shell is undyed. The NPs are free of residual surfactants or free monomers and are either left untreated (hydrophobic) or hydrophobized using $4\ \mu\text{l}$ hexamethyldisilazane (Acros Organics B.V.B. A.) per mg nanoparticles, stirred at 300 rpm for 18 h. These particles were used to prepare water-based nanofluids at volume fractions of $\phi = 0.1\%$ and 1.0% . The surface tension values, measured with a drop tensiometer (Attension, Biolin Scientific), are presented in Table I. The hydrophobized nanofluid exhibited a noticeable decrease in the apparent surface tension compared to the hydrophilic nanofluid. This high surface activity is attributed to the low affinity of hydrophobized NPs for water. A stress-controlled rheometer (MCR702, Anton Paar) with a 50 mm top cone and a 50 mm bottom plate geometry was used to measure the viscosity of the nanofluids, which were all $1\ \text{mPa}\cdot\text{s}$ (shear rate $\dot{\gamma} = 100\ \text{s}^{-1}$, temperature $T = 22\ ^\circ\text{C}$), with the standard deviations within the rheometer torque fluctuation range.

B. Substrates

Smooth glass slides (Thermo Scientific) were chosen as substrates to prevent any contact line pinning due to surface roughness. After cleaning with Milli-Q water and ethanol, the slides were immersed in a dichlorodimethylsilane solution (silanization solution I, Sigma-Aldrich) for 10 min and then allowed to dry. The maximum asperity size, as measured using AFM (supplementary material Fig. S1), is $11.4\ \text{nm}$. The wettability of the modified glass was evaluated with a home-made drop goniometer ($10\ \mu\text{L}$ water drops), with measured contact angle values of 98.6° (static), 107.4° (advancing), and 86.2° (receding).

C. Experimental set-up

The drop dynamics induced by lateral vibration was examined with a home-made experimental device (see Fig. 1), based on a permanent magnet shaker (LSD V201, Brüel & Kjaer, 5 Hz–13 kHz), a high-speed CMOS camera (Phantom Miro C110, 500–1000 fps) equipped with a variable magnification objective (Computar MLM3X-MP), and a back-lighting system to enhance the contrast of side-view drop images. The vibration experiments were performed at 40 Hz and with amplitudes within the range of $20\text{--}160\ \mu\text{m}$. The recorded videos were processed with ImageJ and subsequently analyzed with customized MATLAB codes. The contact angles on the left and right sides were evaluated with a modified version of the MATLAB code of Andersen and Taboryski.²² To analyze the relative displacement of vibrating drops, we used an elliptical fit MATLAB code, provided by Gal.²³

TABLE I. Nanofluid types used in the present experiments with the volume fraction of solids ϕ and the apparent surface tension.

Nanofluid type	ϕ (v/v)	Surface tension (mN/m)
Water	0%	72.2 ± 0.4
Hydrophilic	0.1%	72.5 ± 0.8
Hydrophilic	1.0%	72.9 ± 0.1
Hydrophobized	0.1%	57.2 ± 0.2
Hydrophobized	1.0%	56.4 ± 0.4

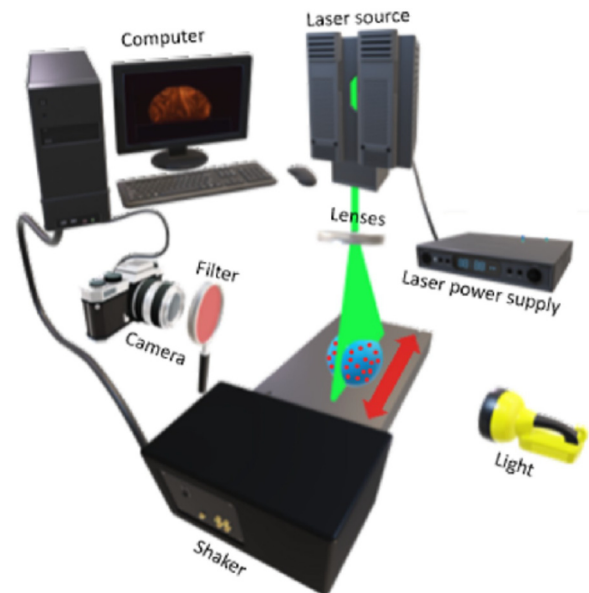


FIG. 1. Set-up for optical and laser visualization of vibrating sessile drops.

Particle image velocimetry was used to visualize the fluid flow within the sessile drops. A set of spherical and cylindrical lenses were adjusted to produce a thin laser sheet ($\sim 0.3\ \text{mm}$ thick) from the laser unit (SDL-532-1500T, Shanghai DreamLaser Technology), precisely focused on the maximum cross section of each sessile drop. This laser sheet acted as an illumination source for the fluorescent NPs suspended within each nanofluid drop. To selectively capture the emitted fluorescent light, we fixed a dichroic filter (FD1R, Thorlabs) to the camera objective. For the experiments performed without nanofluids, we used neutrally buoyant fluorescent polystyrene microparticles ($1.14\ \mu\text{m}$, PS-FluoRed, microparticles GmbH) as tracers, ensuring that the Stokes number, $Stk \ll 1$, indicating that these particles closely follow the fluid flow. The resulting fluorescent signals were analyzed with particle image velocimetry.²⁴ All experiments were conducted at room temperature ($25\ ^\circ\text{C}$) in still air without humidity control. The experimental timescale ($\sim 10\ \text{s}$) was significantly lower than the evaporation timescale ($\sim 20\ \text{min}$ for $5\ \mu\text{L}$ water drops).

III. RESULTS AND DISCUSSION

A. Drop dynamics

On the static substrate, sessile drops of both hydrophilic and hydrophobic nanofluids showed a decrease in contact angle (CA_i) compared to pure water (see Table II and supplementary material Fig. S2). This natural spreading of nanofluids was enhanced as the nanoparticle (NP) concentration increased.²⁰ The surface tension of both nanofluids differs significantly (see Table I), indicating more surface activity of the hydrophobized particles to the air–liquid interface. This reduction leads to a higher spreading coefficient of the hydrophobized nanofluid than the hydrophilic nanofluid on the as-prepared silanized glass substrate. This justifies the higher natural spreading of the hydrophobized nanofluid.

TABLE II. Initial (subscript *i*) and final (*f*) values of contact angle (CA) and contact line length (CLL) for water and the different nanofluids.

Nanofluid type	ϕ (v/v)	CA _{<i>i</i>} (deg)	CA _{<i>f</i>} (deg)	CLL _{<i>i</i>} (mm)	CLL _{<i>f</i>} (mm)
Water	0%	98.6	96.3	2.49	2.53
Hydrophilic	0.1%	95.5	63.2	2.57	3.65
Hydrophilic	1.0%	87.8	62.8	2.64	3.63
Hydrophobized	0.1%	97.6	42.1	2.32	3.91
Hydrophobized	1.0%	84.0	41.9	2.57	3.96

When subjected to the vibrating substrate, no significant migration (movement of the center of mass) of oscillating drops was observed (see Fig. 2). Both the advancing and receding contact angles, however, were altered by the vibration. It is well known that sessile drops, under a suitable mechanical stimulus,³ are relaxed toward the most stable configuration, typically decreasing their contact angle. This effect is referred to as vibration-induced spreading. However, in our study, this forced spreading of nanofluids differed depending on the type of nanofluid, NP concentration, and vibration amplitude. Unlike the pure water drops, the shape of nanofluid drops undergoes continuous flattening during vibration until a steady-state oscillation is observed after approximately 0.5 s for the nanofluid with $\phi = 0.1\%$ hydrophilic particles and more than 8 s for $\phi = 1\%$. As the oscillating contact line dilates, the vertical position of the drop center gradually decreases. Finally, the contact line length of the vibrated nanofluid (CLL_{*f*}) increases under certain conditions (see Table II).

To identify the physical mechanisms responsible for drop spreading, we estimate the ratio between inertia forces and capillary forces via the Weber number,

$$We = \frac{\rho v_p^2 2r_c}{\gamma_{lv}}, \quad (1)$$

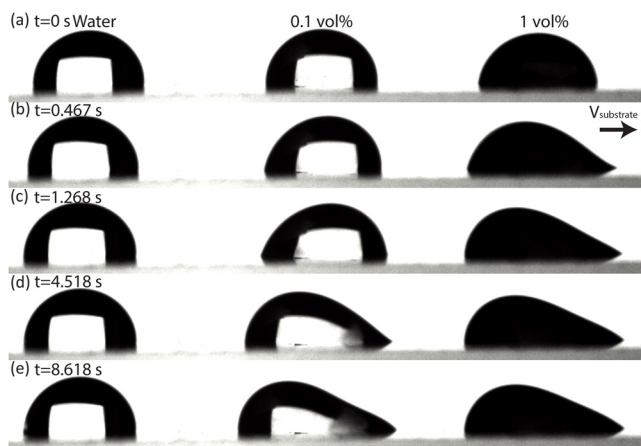


FIG. 2. (a)–(e) Image sequence of 5 μL (left) water and hydrophilic nanofluid drops with (center) 0.1 vol. % and (right) 1 vol. % solid loading during the substrate vibration. The images are taken at the same point in the period, with the arrow indicating the direction of substrate motion in all the images.

where ρ represents the liquid density, v_p is the maximum linear velocity of the substrate (i.e., the product between the oscillating frequency and amplitude), r_c is the contact drop radius, and γ_{lv} is the surface tension (liquid–vapor). For the highest amplitude vibration, the highest NP concentration of 1%, and the lowest nanofluid surface tension, the results obtained in our experiments held $We \ll 1$. This observation indicates that the interfacial forces dominate for drop spreading over the vibration. The same analysis is completed for the small viscous forces at the contact line (via the capillary number). Definitely, the vibrational input acts as an energy trigger, bringing the system closer to the present interfacial thermodynamic equilibrium.

We illustrate in Fig. 3(a) the identified spreading regimes with the most meaningful data (obtained with the vibration amplitude 75 μm). In the case of pure water drops, the contact line (and contact angle) oscillates in a steady regime around their equilibrium values. However, the nanofluid drops oscillate with a preferential advancing motion up to a new equilibrium configuration. The stabilization kinetics of oscillating nanofluid drops varies as the NP concentration, although for each nanofluid the contact line length reaches the same value. The evolution of advancing and receding contact angles during spreading is reported in the supplementary material (see Fig. S3).

In terms of the drop center position and the substrate position during vibration [Fig. 3(b)], a series of evolving ellipses reveal the phase shift (ellipse rotation) between the oscillating deformable drop and the driving substrate. For an in-phase rigid body, this graph should represent an inclined straight line, with a slope related to the amplitude ratio. The phase shift [Fig. 3(c)] for the water drop is consistent since its oscillating behavior remained unchanged during substrate vibration. On the other hand, the contact area gradually increased during vibration for the nanofluid drops. This affects the lateral oscillation of the drop center, resulting in a continuous phase change of the drop oscillation with respect to the substrate. The phase shift correlates with the rate of energy transfer between the oscillating drop and driving substrate.

The ellipse area provides an estimate of the global performance of the driven drop oscillation [Fig. 3(d)]. In many oscillating mechanical systems, the fastest energy transfer is reached when the driving force and the system are precisely 90° out of phase. This feature is highlighted with dashed lines in Figs. 3(c) and 3(d). The hydrophobized nanofluid showed a similar behavior to the hydrophilic nanofluid, but a higher vibration level was required to initiate the forced spreading. This could be caused by the lower restoring cohesive force of the hydrophobized nanofluid. However, it might be mostly attributed to the collective behavior of the hydrophobized NPs within the oscillating drops. When water drop and substrate oscillate 90° out of phase, the maximum shear adhesion force may be readily overcome and the drop describes a rocking translational motion. In the supplementary material, the corresponding graphs for hydrophobized nanofluids are included for completeness.

B. Internal flow in nanofluid drops

To explain the differences found in Sec. III A, a visualization of the fluid flows formed within the nanofluid drops is useful. Therefore, we observed the fluid velocity field in oscillating water drops, by using diluted fluorescent microparticles [Fig. 4(a)]. The applied vibration induces a complex three-dimensional internal flow within the droplet. By focusing our analysis on the droplet’s middle section, parallel to the

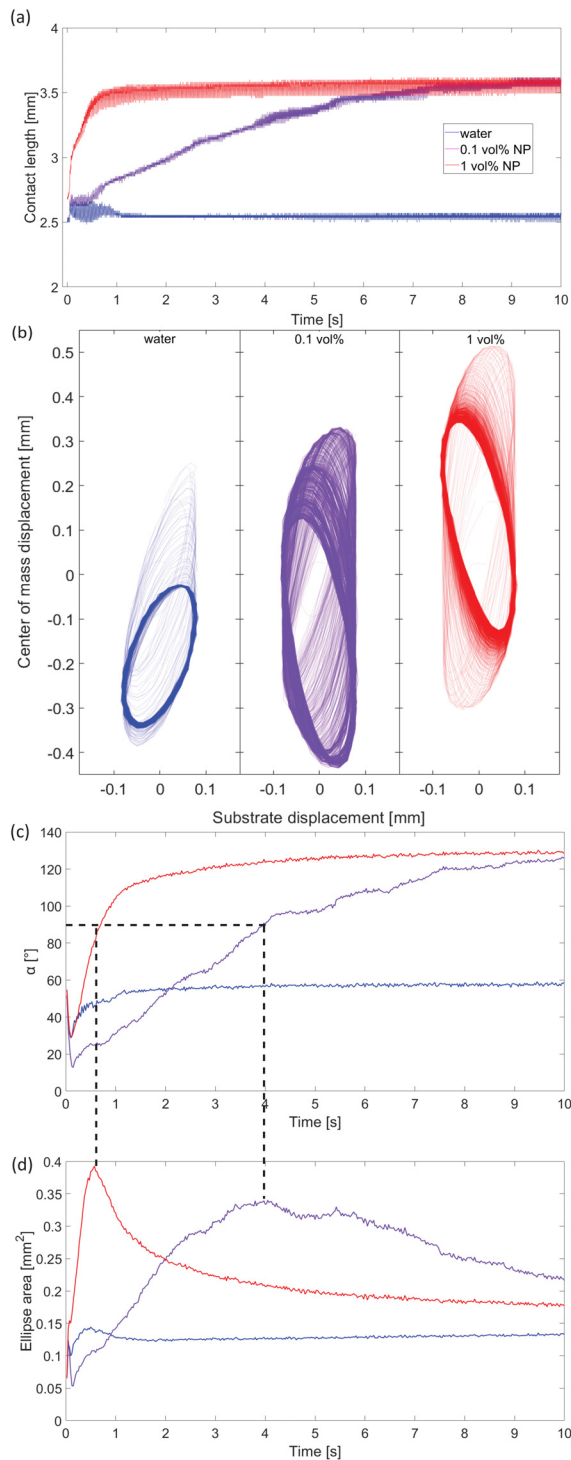


FIG. 3. (a) Contact length, (b) lateral position of the drop center with respect to the substrate position for (left) water, (center) 0.1% hydrophilic and (right) 1.0% hydrophilic nanofluid drops, (c) phase shift of the drop-substrate oscillations, and (d) ellipse area per oscillation cycle in terms of time. The 90°-phase situations are located with dashed lines.

direction of vibration, we identified two alternating asymmetrical vortices. Close to the surface, within the Stokes boundary layer,²⁵ the flow patterns were found to align with the lateral motion of the oscillating substrate.

For the sake of clarity, we show in Figs. 4(b) and 4(c) the NP distribution within the nanofluid drops under conditions of low vibration amplitude. The formation of well-defined zones within the drops, characterized by stronger fluorescent signals, reveals localized NP concentrations.²⁶ The hydrophilic NPs were evenly distributed around the vortices, forming disk-shaped zones with high concentration. In contrast, the hydrophobized NPs accumulated at the stagnation points of the vortices but they also followed the outer streamlines, directed toward the solid-liquid interface. Unlike the hydrophilic NPs, the surface active NPs diffused from the drop bulk. Since the two types of

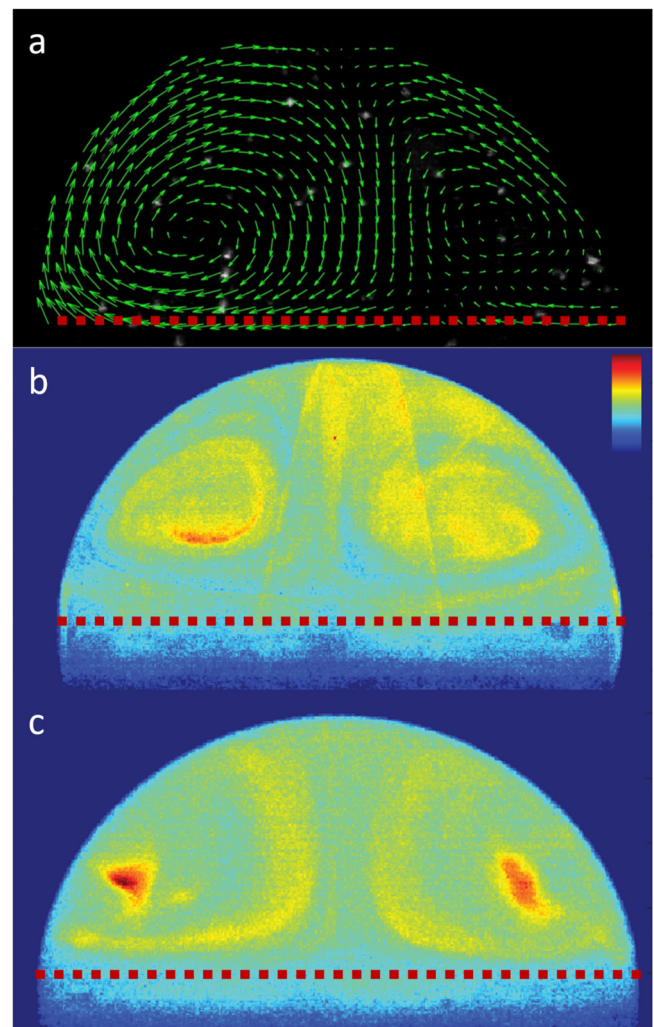


FIG. 4. (a) Velocity field inside an oscillating water drop. Concentration field of NPs within oscillating drops containing (b) hydrophilic and (c) hydrophobized nanofluid (0.1 v/v%). The red color reveals greater NP density values and the blue color, lower values. The stagnant points can be identified at each vortex center. The red dashed lines indicate the position of the substrate.

21 June 2024 10:14:29

nanofluid were differently dispersed in bulk, the fluid flow might transport different amounts of NPs toward the fresh solid–liquid interface. This allows us to assume that the deposition of hydrophobized NPs onto the substrate was favored. Despite the present evidence of substrate modification observed in the differences between water and nanofluid drops in the final contact angles (see Table II) and the stabilization in the contact line spreading, additional experiments are conducted to obtain direct evidence of substrate modification [see the supplementary material Figs. S5(a)–S5(c)].

C. Spreading triggering

We have identified three distinct spreading regimes based on the spreading rate: null, slow, and fast. We plot in Fig. 5(a) the comprehensive spreading diagram for both types of nanofluid, in terms of the NP concentration and vibration amplitude. The gray area denotes conditions where no drop spreading was observed, the shaded region corresponds to the spreading onset, with slow dynamics (~10 s), and the white area points out to the rapid spreading (~1 s).

It is well known that the introduction of NPs into sessile water drops leads to two main competing effects:¹⁸ self-pinning and natural spreading, but at different timescales. Spreading of free nanofluid drops is a slow dynamic process, and its rate is magnified by concentration. The solid–liquid interfacial energy, γ_{sl} is altered by NP adsorption/deposition;¹⁸ consequently, the equilibrium contact angle, defined by the Young equation, is determined by this modified surface and the new γ_{sl} value. The presence of NPs also increases the surface roughness with nanoasperities.^{18,27} These alterations in the substrate properties during vibration influence the drop’s equilibrium condition. At the start of the vibration cycle, the nanofluid drops oscillate around out-of-equilibrium configurations. For each vibration cycle, the drop contact line slips and deposits NPs onto the newly formed solid–liquid interface. The onset of the contact line motion then requires higher

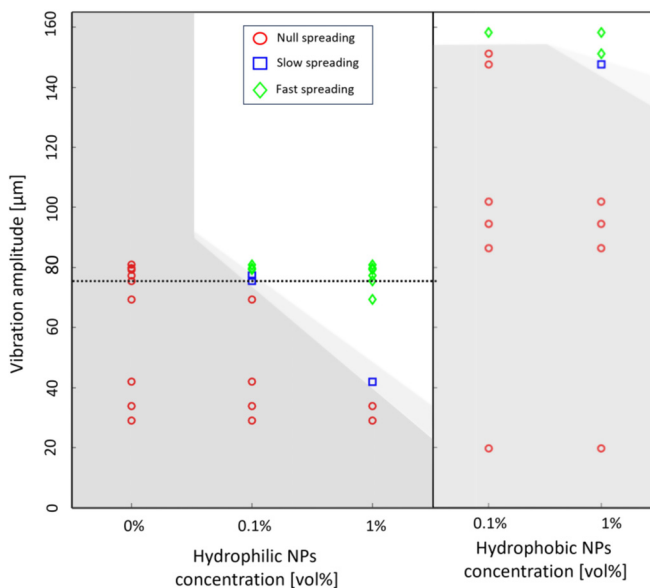


FIG. 5. Drop spreading diagrams for (left) hydrophilic and (right) hydrophobized nanofluids. The dashed line indicates the vibration amplitude used in Fig. 3.

threshold forces to overcome self-pinning, preventing dewetting during the receding mode. An elongated contact area was consolidated after each cycle. After several cycles, the nanofluid drop is able to attain a steady oscillation [Fig. 3(a)] and the forced spreading ceases. The self-pinning effect is achieved with a large number of NPs adsorbed at the newly created solid–liquid interface. To attain this threshold value, either more vibration cycles are required at low concentrations or a fewer cycles at higher concentration of the nanofluid. A final balance is attained between the enhanced retention force and the restoring force. This explanation is supported by the trends observed in Fig. 3, where each nanofluid at different concentrations reaches the same final value of the contact line length (see Table II), i.e., the same final saturation of the solid–liquid interface. Self-pinning is also rationalized in terms of higher energy barriers that separate the multiple metastable drop configurations.

To further elucidate these observations, Fig. 6 visually represents the different energy configurations between nanofluid drops and water drops on solid substrates. This figure highlights how the presence of nanoparticles modifies the energy landscape due to altered surface roughness and interfacial energy, as a direct consequence of nanoparticle adsorption and deposition. The preferential adsorption at interfaces of hydrophobized NPs increases the self-pinning force and decreases the capillary restoring force. This justifies that the drop spreading for the hydrophobized nanofluid is only triggered at high concentration and high vibration amplitude. Without such drop vibration, the NPs typically only accumulate at the three-phase contact lines driven by the convective flows. To model the fundamental behaviors of nanofluid droplet spreading, we have developed a heuristic mechanical model.²⁸ This model is detailed in the supplementary material Fig. S6.

IV. CONCLUSIONS

The dynamics of nanofluid sessile drops on laterally vibrating substrates is significantly different from that of pure water drops. The incorporation of hydrophilic and hydrophobized nanoparticles affects the drop spreading process under external vibration. Through the analysis of the drop center oscillation for various vibration amplitudes and nanoparticle concentrations, we have identified three unique spreading regimes. The preferential adsorption of hydrophobic nanoparticles at interfaces enhances contact line pinning and reduces the restoring force (surface tension). This produces an increase in the

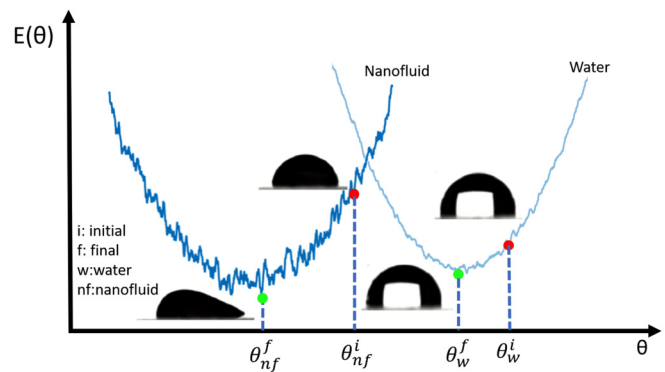


FIG. 6. Energy configuration for water and nanofluid drops on solid substrates, illustrating the impact of nanoparticle deposition on the equilibrium states.

threshold amplitude for nanofluid drop spreading. To gain deeper understanding, we employed laser-induced fluorescence visualization to assess the nanofluid internal flows, revealing the relevant impact of hydrophobic interactions on the nanoparticle concentration profiles, particularly around the vortex stagnant points. Driven by these internal flows, the nanoparticles deposit onto the solid-liquid interface, modifying the substrate in terms of both roughness and interfacial energy and thereby effectively altering the substrate wetting properties. This research unveils the underlying mechanisms for vibration-triggered spreading of nanofluid drops, offering valuable parameters for tailoring liquid manipulation. This research opens new possibilities for the tunable deposition of nanoparticles on substrates and also has implications for applications of nanofluids where such a deposition may have undesirable implications.

SUPPLEMENTARY MATERIAL

See the supplementary material for enhances the findings of the main text with additional visual and graphical data. It includes initial images of contact angles for different nanofluids, atomic force microscopy topography of the substrate, and analyses of contact angle dynamics. Additional results cover the dynamics of hydrophobized nanofluid drops under vibration, showing changes in contact line dynamics and displacement patterns. Visual evidence of nanoparticle deposition on the substrate and a theoretical model of the mechanical interactions within vibrating nanofluid drops are also provided. These materials offer a deeper understanding of the experimental outcomes and theoretical insights presented in the manuscript.

ACKNOWLEDGMENTS

This project has received funding from the European Union's Horizon 2020 research and innovation programme under the Marie Skłodowska-Curie Grant Agreement No. 955612. The UGR co-authors are also grateful to project PID2020-116082GB-I00 funded by MCIN/AEI/10.13039/501100011033.

AUTHOR DECLARATIONS

Conflict of Interest

The authors have no conflicts to disclose.

Author Contributions

Schon Fusco and Lingyue Liu equally contributed to this work.

Schon Gabriel Fusco: Data curation (equal); Investigation (equal); Software (equal); Visualization (equal); Writing – original draft (equal). **Lingyue Liu:** Conceptualization (equal); Investigation (equal); Methodology (equal); Visualization (equal). **MA Cabrerizo-Vilchez:** Funding acquisition (lead); Methodology (equal). **Erin Koos:** Funding acquisition (equal); Project administration (equal); Supervision (supporting); Writing – review & editing (equal). **Miguel Rodríguez-Valverde:** Conceptualization (equal); Project administration (equal); Supervision (lead); Writing – review & editing (equal).

DATA AVAILABILITY

The data that support the findings of this study are available within the article and its supplementary material.

REFERENCES

- ¹E. Bormashenko, R. Pogreb, G. Whyman, Y. Bormashenko, and M. Erlich, "Vibration-induced Cassie-Wenzel wetting transition on rough surfaces," *Appl. Phys. Lett.* **90**, 201917 (2007).
- ²X. Noblin, R. Kofman, and F. Celestini, "Ratchetlike motion of a shaken drop," *Phys. Rev. Lett.* **102**, 194504 (2009).
- ³M. A. Rodríguez-Valverde, F. J. Montes Ruiz-Cabello, and M. A. Cabrerizo-Vilchez, "A new method for evaluating the most-stable contact angle using mechanical vibration," *Soft Matter* **7**, 53 (2011).
- ⁴N.-T. Nguyen and Z. Wu, "Micromixers—A review," *J. Micromech. Microeng.* **15**, R1 (2005).
- ⁵Y. Lee, G. Amberg, and J. Shiomi, "Vibration sorting of small droplets on hydrophilic surface by asymmetric contact-line friction," *PNAS Nexus* **1**, pgac027 (2022).
- ⁶S. Daniel, M. K. Chaudhury, and P.-G. De Gennes, "Vibration-actuated drop motion on surfaces for batch microfluidic processes," *Langmuir* **21**, 4240 (2005).
- ⁷D. Sun and K. F. Böhringer, "An active self-cleaning surface system for photovoltaic modules using anisotropic ratchet conveyors and mechanical vibration," *Microsyst. Nanoeng.* **6**, 87 (2020).
- ⁸M. Trapuzzano, A. Tejada-Martínez, R. Guldiken, and N. Crane, "Volume and frequency-independent spreading of droplets driven by ultrasonic surface vibration," *Fluids* **5**, 18 (2020).
- ⁹J. D. Whitehill, A. Neild, and M. H. Stokes, "Forced spreading behavior of droplets undergoing low frequency vibration," *Colloids Surf. A* **393**, 144 (2012).
- ¹⁰E. L. Decker and S. Garoff, "Using vibrational noise to probe energy barriers producing contact angle hysteresis," *Langmuir* **12**, 2100 (1996).
- ¹¹X. Noblin, A. Buguin, and F. Brochard-Wyart, "Vibrated sessile drops: Transition between pinned and mobile contact line oscillations," *Eur. Phys. J. E* **14**, 395 (2004).
- ¹²J. Whitehill, A. Neild, T. W. Ng, and M. Stokes, "Collection of suspended particles in a drop using low frequency vibration," *Appl. Phys. Lett.* **96**, 053501 (2010).
- ¹³A. Neild, S. Oberti, G. Radziwill, and J. Dual, "Simultaneous positioning of cells into two-dimensional arrays using ultrasound," *Biotechnol. Bioeng.* **97**, 1335 (2006).
- ¹⁴A. Neild, S. Oberti, and J. Dual, "Design, modeling and characterization of microfluidic devices for ultrasonic manipulation," *Sens. Actuators B* **121**, 452 (2007).
- ¹⁵J. L. Han, H. Hu, Q. Y. Huang, and Y. L. Lei, "Particle separation by standing surface acoustic waves inside a sessile droplet," *Sens. Actuators A* **326**, 112731 (2021).
- ¹⁶K. Sefiane, J. Skilling, and J. MacGillivray, "Contact line motion and dynamic wetting of nanofluid solutions," *Adv. Colloid Interface Sci.* **138**, 101 (2008).
- ¹⁷Y. T. Aksoy, L. Liu, M. Abboud, M. R. Vetrano, and E. Koos, "Role of nanoparticles in nanofluid droplet impact on solid surfaces," *Langmuir* **39**, 12 (2023).
- ¹⁸Y. Jiang, W. Xu, and C.-H. Choi, "Effects of particulates on contact angles and adhesion of a droplet: A critical review," *Rev. Adhes. Adhes.* **4**, 192 (2016).
- ¹⁹D. Noguera-Marín, C. L. Moraila-Martínez, M. A. Cabrerizo-Vilchez, and M. A. Rodríguez-Valverde, "In-plane particle counting at contact lines of evaporating colloidal drops: Effect of the particle electric charge," *Soft Matter* **11**, 987 (2015).
- ²⁰K. Kondiparty, A. Nikolov, S. Wu, and D. Wasan, "Wetting and spreading of nanofluids on solid surfaces driven by the structural disjoining pressure: Statics analysis and experiments," *Langmuir* **27**, 3324 (2011).
- ²¹L. Liu, J. Allard, and E. Koos, "Enhanced contact flexibility from nanoparticles in capillary suspensions," *J. Colloid Interface Sci.* **665**, 643 (2024).
- ²²N. K. Andersen and R. Taboryski, "Drop shape analysis for determination of dynamic contact angles by double sided elliptical fitting method," *Meas. Sci. Technol.* **28**, 047003 (2017).
- ²³O. Gal, see https://www.mathworks.com/matlabcentral/fileexchange/3215-fit_ellipse for "fit_ellipse" (2024).
- ²⁴W. Thielicke and R. Sonntag, "Particle image velocimetry for MATLAB: Accuracy and enhanced algorithms in PIVlab," *J. Open Res. Software* **9**, 12 (2021).

- ²⁵L. Dong, A. Chaudhury, and M. Chaudhury, "Lateral vibration of a water drop and its motion on a vibrating surface," *Eur. Phys. J. E* **21**, 231 (2006).
- ²⁶U. Unnikrishnan and V. Yang, "A review of cooling technologies for high temperature rotating components in gas turbine," *Propul. Power Res.* **11**, 293 (2022).
- ²⁷S. Lim, H. Horiuchi, A. D. Nikolov, and D. Wasan, "Nanofluids alter the surface wettability of solids," *Langmuir* **31**, 5827 (2015).
- ²⁸Y. Dong, H. R. Holmes, and K. F. Böhringer, "Converting vertical vibration of anisotropic ratchet conveyors into horizontal droplet motion," *Langmuir* **33**, 10745 (2017).